Polariton theory of first-order Raman scattering in finite crystals for transparent and absorbing frequency regions*

Roland Zeyher,† Chin-Sen Ting,‡ and Joseph L. Birman§
Physics Department, New York University, New York, New York 10003
(Received 9 April 1973; revised manuscript received 30 January 1974)

A new treatment is given of first-order Raman scattering in bounded insulators using the polariton picture. A novel feature of the work is the use of polariton states which have the correct asymptotic behavior as incoming or outgoing photons in the region exterior to the crystal, and are properly matched, via boundary conditions to the usual polaritons (coupled exciton-photon states) in the region interior. We recover in this polariton treatment, essentially the results of lowest-order perturbation theory for the scattering cross section with some significant modifications in part depending on whether allowed or forbidden exciton-phonon interaction is involved. *Inter alia* our work shows that the exterior-photon density-of-states factors appear in the cross section thereby resolving previous uncertainty regarding use of polariton group or energy velocities in the absorption region. Calculations are given of frequency dependence of Raman-scattering cross sections for incident frequencies below and above the energy gap, for allowed and forbidden electron-phonon coupling, and for correlated (exciton) and Bloch (free) electron-hole pairs. These are compared with experiment for CdS and GaP.

I. INTRODUCTION

This paper has two parts which are interdependent. In the first part we shall give a theory of Raman scattering by phonons in a bounded crystal using the polariton picture. For reasons to be described below we believe this treatment is an improvement over previous work using the polariton picture since our theory gives a unified account of all the fields external and internal to the crystal. In the second part of this paper we calculate the frequency dependence of the one-phonon Raman scattering cross section for frequencies above and below the band gap of an insulator. Our calculation considers both allowed and forbidden scattering (involving deformation and Frohlich electron-lattice interactions) and also free (Bloch) and exciton (Wannier) electron-hole pairs. Our explicit calculation for the combination of Wannier excitons—allowed and forbidden scattering with incident frequencies above the gap (in the "continuum") is new. We give numerical results and compare our calculation with experimental results in GaP and CdS. At various places in the text we shall compare our results with earlier treatments which used a Bloch-electron picture[1] or an exciton picture,[2] both treated in perturbation theory, or other treatments using polariton picture.[3-9]

In the polariton quasiparticle picture the basic entity which plays the dynamic role in Raman scattering is the coupled exciton-photon mode: the polariton. This picture is traditionally applied to phonon Raman scattering as follows. The incident external photon ω is assumed to create an initial exciton-polariton within the crystal which scatters to a final exciton polariton with production of a phonon or phonon polariton (the latter if final-state interactions are important). The final exciton polariton upon impinging on the bounding surface produces the scattered external photon ω'. It is clear that to compare the measured cross section for scattering of an external photon ω to an external photon ω' with that calculated on this picture proper account must be taken of the process by which the incident photon becomes the initial polariton, and the final polariton becomes the scattered photon, i.e., transmission across the bounding surfaces of the medium. In the traditional treatments in the polariton picture this is done as follows.

First a cross section $(\partial^2\sigma/\partial\Omega\partial\omega')_I$ is calculated, say, for a crystal of unit volume, which describes scattering of polaritons inside the crystal for which we use subscript I. Then, to account for transmission coefficients, absorption corrections, etc., one can follow Loudon's procedure.[1] For example, in the case of back scattering at normal incidence from a semi-infinite crystal one has the relation

$$\frac{\partial^2\sigma}{\partial\Omega\,\partial\omega'} = \left(\frac{\partial^2\sigma}{\partial\Omega\,\partial\omega'}\right)_I T(\omega)T(\omega')\frac{F}{\kappa(\omega)+\kappa(\omega')}\,. \tag{1}$$

$T(\omega)$ is the Maxwell transmission coefficient at the incident frequency ω; ω' is the scattered frequency; F is the illuminated area; and $\kappa(\omega)$ is the imaginary part of the refractive index at frequency ω. $1/[\kappa(\omega)+\kappa(\omega')]$ can be interpreted as a skin depth and $F/[\kappa(\omega)+\kappa(\omega')]$ as an effective scattering volume. The essential point of Eq. (1) is that there is a factorization of the

calculated "measured" cross section into a factor representing polariton scattering processes interior to the crystal times the transmission factors at the boundary.

This conventional procedure needs improvement for several reasons. First of all, it would be preferable to treat the eigenmodes of the entire inhomogeneous system (bounded crystal plus vacuum) on a unified footing rather than establish a dichotomy between exterior photons and interior polaritons, which is only *a posteriori* rectified by joining the two via transmission factors. Secondly, from Eq. (1) it is apparent that the linewidth of the scattered radiation should be partially due to the linewidth (lifetime) of the final exciton-polariton state. Hence the scattered linewidth would be expected to increase as the incident frequency approached a discrete exciton line. But this expectation is contradicted by all the experimental evidence, which indicates that the scattered linewidth is essentially that due to final phonon lifetime, i.e., produced by phonon anharmonicity. A final matter concerns the uncertainty regarding exactly which velocity of the polariton quasiparticle should be used in the calculated cross section $(\partial^2\sigma/\partial\Omega\,\partial\omega')_I$. There seems no agreement on this point, with various authors using group or energy transport velocities; in either event these velocities are imprecise in the region of (exciton) absorption. We believe the treatment of polariton Raman scattering which we developed is free of these deficiencies.

Our work is based on the construction of the correct eigenmodes for the polariton Hamiltonian in the bounded system. These modes have the property that in the interior region within the crystal they are the familiar coupled exciton polariton, and in the exterior region they are the true asymptotic scattering states, namely, bare photons, with both parts correctly joined by the full set of necessary boundary conditions (including the additional boundary conditions if spatial dispersion is taken into account). In Sec. II we obtain these modes by starting from the polariton Hamiltonian consisting of free photons (in both exterior and interior regions) and free excitons plus the bilinear exciton-photon interaction (interior region). The diagonalization of this Hamiltonian is equivalent to the solution of Maxwell's equations in a medium with a prescribed (and in general nonlocal) susceptibility, and produces the proper eigenmodes. Also in Sec. II we give the trilinear exciton-phonon interaction. The total Hamiltonian is the sum of all the above-mentioned constituent parts.

In Sec. III we define the total cross section which is to be compared with experiment. This cross section depends upon the matrix elements of a T operator which contains both the exciton-photon and exciton-phonon interactions. We modify a standard textbook discussion of particle scattering from two potentials to deal with this case. The asymptotic states which are scattered from the two potentials are bare (exterior) photons, and these photons define the incident flux and the density of final states. Using an operator identity the exciton-photon interaction can be removed from the T operator if the asymptotic bare photon states are simultaneously renormalized by the exciton-photon interaction. But these renormalized bare photon states are exactly the polariton modes introduced in Sec. II, satisfying asymptotically incoming or outgoing wave boundary conditions. This transformation then permits us to write the transition matrix element in a form of a transition between polariton modes produced by the exciton-phonon interaction.

If spatial dispersion is neglected the calculated cross section can then be factorized into a product of a Raman tensor times a "structure factor," formally similiar to Eq. (1). The structure factor accounts for transmission and absorption effects. In Sec. IV this is worked out for the case of normal incidence on a semi-infinite crystal. We find that the formal expression for the Raman tensor agrees with that obtained by using lowest order perturbation theory on bare exciton and bare photon states, with the important difference that all momenta in the resulting expressions refer to polariton momenta in the crystals and not to bare photon momenta. In summary this result shows that even in the polariton description the correct $(\partial^2\sigma/\partial\Omega\,\partial\omega')_I$ is that of lowest-order perturbation theory with the aforementioned changes. Also the vacuum velocity of light (the asymptotic state) replaces the polariton velocity in the formulas; the width of the scattered light is due to phonon lifetime (anharmonicity) effects and generally damping effects arise in a straightforward fashion; finally the transmission coefficients occur directly and do not need to be put into the scattering formulas in an *a posteriori* or *ad hoc* fashion. In this way our result removes the difficulties with conventional polariton theories referred to earlier. In the Appendix we generalize the work to include spatial dispersion by including center of mass motion of a 1*s* exciton.

In the second part of this paper we use these results to explicitly calculate some cases of current interest for incident frequencies very near a discrete exciton or in the electron-hole continuum. In the latter case (frequencies in the continuum) one must take into account the imaginary part of the Raman tensor.[10-14] The cross section is then

proportional to the sum of the squared real part plus the squared imaginary part of the Raman tensor. In Sec. V we evaluate the Raman tensor for the four different cases relevant to experiment; namely, with intermediate state either free (Bloch) electron-hole pairs, or Wannier excitons and with the exciton-phonon interaction either $\vec{q}$-independent ("allowed scattering") or $\vec{q}$-dependent Frohlich interaction ("forbidden scattering"). Note that our results imply that apart from the refractive index as a multiplicative factor in case of intraband Frohlich scattering, the perturbation results for the other cases (deformation potential and interband Frohlich) can be taken over without change. Allowed scattering has been considered in Refs. 15–17. For the Wannier exciton case we give an analytic expression for the Raman tensor including the imaginary part which has not been previously given. A calculation for forbidden scattering with free electron-hole pairs has been reported by Hamilton.[18] We were not able to reproduce his results for first-order scattering and we believe them incorrect. The calculation for forbidden scattering via Wannier excitons[19] for incident frequencies above the band gap is reported here for the first time. Actual numerical calculations are given here, for several ranges of (material) parameters, and compared with experiment in Sec. VI.

II. HAMILTONIAN

The first step is to write the total Hamiltonian for a bounded crystal. The Hamiltonian consists of free photon, exciton, and phonon fields plus the bilinear exciton-photon and trilinear exciton-phonon couplings.[2] We shall not discuss the justification for using this Hamiltonian since that is well known.[1,2]

The total Hamiltonian H can be split into a polariton part H^{Pol}, a (harmonic) phonon part H^L, and exciton-phonon interaction H':

$$H = H^{\mathrm{Pol}} + H^L + H', \tag{2}$$

$$\begin{aligned} H^{\mathrm{Pol}} = & \sum_{\vec{k},\gamma} \hbar c|\vec{k}|(\hat{a}^\dagger_{\vec{k}\gamma}\hat{a}_{\vec{k}\gamma} + \tfrac{1}{2}) + \sum_i \hbar\omega_i(\hat{b}^\dagger_i \hat{b}_i + \tfrac{1}{2}) \\ & + i\sum_{i,\vec{k},\gamma} g_{i,\vec{k}\gamma}\left(\frac{2\pi\hbar\omega_i}{c|\vec{k}|}\right)^{1/2}\hat{b}_i(\hat{a}^\dagger_{\vec{k}\gamma} + \hat{a}_{-\vec{k}\gamma}) + \text{c.c.} \\ & + \sum_{\vec{k},\gamma}\frac{\omega_p^2}{|\vec{k}|}\frac{\hbar}{4c}(\hat{a}^\dagger_{\vec{k}\gamma} + \hat{a}_{-\vec{k}\gamma})(\hat{a}^\dagger_{-\vec{k}\gamma} + \hat{a}_{\vec{k}\gamma}), \end{aligned} \tag{3}$$

$$H^L = \sum_{\vec{q}} \hbar\Omega(\vec{q})(\hat{c}^\dagger_{\vec{q}}\hat{c}_{\vec{q}} + \tfrac{1}{2}), \tag{4}$$

$$H' = \sum_{i,j,\vec{q}} f_{ij}(\vec{q})\hat{b}^\dagger_i \hat{b}_j \hat{c}^\dagger_{\vec{q}} + \text{c.c.} \tag{5}$$

$\hat{a}^\dagger_{\vec{k}\gamma}$, $\hat{b}^\dagger_i$, $\hat{c}^\dagger_{\vec{q}}$ are creation operators for photon, exciton, and phonon, respectively. $\vec{k}$ denotes the momentum of the photon and γ a polarization label; i and $\vec{q}$ are quantum labels which characterize the exciton and phonon states for a bounded crystal, respectively. The exciton label i consists of quantum numbers for the relative and center-of-mass motion of the exciton as well as of band indices for the electron and hole band. We use periodic boundary conditions for the phonons, which can then be characterized by a quasimomentum $\vec{q}$ and a branch index; the latter is always omitted in the following.

In Eq. (3), $g_{i,\vec{k}}$ is the bilinear exciton-photon coupling coefficient, which can be expressed as matrix element $\langle i|\vec{A}_{\vec{k}}\cdot\vec{p}|0\rangle$, where $|i\rangle$ is the exciton state; $|0\rangle$ is the ground state, with no exciton present; $\vec{A}_{\vec{k}}$ is the vector potential for photon $\vec{k}$; $\vec{p}$ is the relevant momentum operator. We do not require detailed specification of this matrix element but we shall implicitly assume that the optical transition $0 \to i$ is dipole allowed; in case it is forbidden higher order terms will enter. The exciton-phonon coupling coefficient $f_{ij}(\vec{q})$ in Eq. (5) will be discussed in Sec. II B.

It may not be superfluous to remark that the bare exciton and phonon fields exist only in the interior of the crystal, and likewise their couplings to the photon as well as to each other, while the bare photon is assumed to exist in both the interior and exterior regions. We now turn to the polariton Hamiltonian and its eigenstates.

A. Polariton Hamiltonian

H^{Pol} is a bilinear form in the photon and exciton operators, and can therefore be diagonalized by a linear transformation to give

$$H^{\mathrm{Pol}} = \sum_{\vec{k}_0,\gamma} \hbar c|\vec{k}_0|\hat{B}^\dagger_{\vec{k}_0\gamma}\hat{B}_{\vec{k}_0\gamma}. \tag{6}$$

The vacuum state $|0\rangle$ state of H^{Pol} is defined by $\hat{B}_{\vec{k}\gamma}|0\rangle = 0$ for all $\vec{k}_0$ and γ. Note that we use the label $\vec{k}_0$ of the external photon to label the polariton state. We shall discuss this more fully below, and also later for the scattering cross section we shall need to specify asymptotic "incoming" and "outgoing" photon states and we shall then affix label "in" and "out" to the $\hat{B}^\dagger$ and $\hat{B}$ operators. We restrict our discussion to cubic crystals with transverse polarization waves.

The operators $\hat{B}$ are linear combinations of the $\hat{a}$ and $\hat{b}$ operators. It is convenient for the following to begin with linear combinations of the $\hat{a}$ and $\hat{b}$ operators which correspond to the classical field and momentum variables:

$$\hat{A}_{\vec{k}\gamma}=\frac{\hat{a}^{\dagger}_{\vec{k}\gamma}+\hat{a}_{-\vec{k}\gamma}}{(c|\vec{k}|)^{1/2}}\ ,\quad \hat{P}_{\vec{k}\gamma}=i(c|\vec{k}|)^{1/2}(\hat{a}^{\dagger}_{\vec{k}\gamma}-\hat{a}_{-\vec{k}\gamma}),\tag{7}$$

$$\hat{\alpha}_i=\frac{\hat{b}_i+\hat{b}_i^{\dagger}}{(\omega_i)^{1/2}}\ ,\quad \hat{\Pi}_i=i(\omega_i)^{1/2}(\hat{b}_i^{\dagger}-\hat{b}_i).\tag{8}$$

In terms of these auxiliary operators, we write the $\hat{B}^{\dagger}$ operator as

$$\hat{B}^{\dagger}_{\vec{k}_0\gamma}=\sum_{\vec{k}\,\gamma'}(A^{\vec{k}_0\gamma}_{\vec{k}'\gamma'}\hat{A}_{\vec{k}'\gamma'}+P^{\vec{k}_0\gamma}_{\vec{k}'\gamma'}\hat{P}_{\vec{k}'\gamma'})+\sum_i(\alpha_i^{\vec{k}_0\gamma}\hat{\alpha}_i+\Pi_i^{\vec{k}_0\gamma}\hat{\Pi}_i)\ ,\tag{9}$$

and likewise for the Hermitian adjoint. Scalar amplitudes are written everywhere without caret, the corresponding operators are written with a caret. To find the correct linear combinations (9) we need to use the equation of motion

$$i\hbar\dot{\hat{B}}^{\dagger}_{\vec{k}_0\gamma}=[\hat{B}^{\dagger}_{\vec{k}_0\gamma},\ H^{\mathrm{Pol}}]=\hbar c|\vec{k}_0|\hat{B}^{\dagger}_{\vec{k}_0\gamma}=\hbar\omega\hat{B}^{\dagger}_{\vec{k}_0\gamma}\ .\tag{10}$$

This can be written as a system of equations for the scalar amplitudes

$$i\omega_i^2\Pi_i-\omega\alpha_i=0\ ,\tag{11}$$

$$-i\omega P_{\vec{k}'\gamma'}+A_{\vec{k}'\gamma'}=0\ ,\tag{12}$$

$$(\omega_i^2-\omega^2)\alpha_i=2i\frac{\omega_i^2}{\omega}\left(\frac{2\pi}{\hbar}\right)^{1/2}\sum_{\vec{k}'\gamma'}g_{i,\vec{k}'\gamma'}A_{\vec{k}'\gamma'},\tag{13}$$

$$(-\omega^2+c^2k'^2+\omega_p^2)A_{\vec{k}'\gamma'}=-2i\omega\left(\frac{2\pi}{\hbar}\right)^{1/2}\times\sum_i g_{i,-\vec{k}'\gamma'}\alpha_i\ .\tag{14}$$

Inserting Eq. (13) into (14) gives

$$\{-\omega^2+c^2k^2+\omega_p^2\}A_{\vec{k}\gamma}=\frac{8\pi}{\hbar}\times\sum_{i,\vec{k}'\gamma'}\frac{g_{i,-\vec{k}'\gamma'}g_{i,\vec{k}'\gamma'}}{\omega_i^2-\omega^2}\omega_i^2A_{\vec{k}'\gamma'}.\tag{15}$$

For simplicity here we drop the superscript $(\vec{k}_0\gamma)$ on $A^{\vec{k}_0\gamma}_{\vec{k}'\gamma'}$, $P^{\vec{k}_0\gamma}_{\vec{k}'\gamma'}$, $\alpha_i^{\vec{k}_0\gamma}$, and $\Pi^{\vec{k}_0\gamma}$ defined from Eq. (9). The quantum label i for the exciton can be decomposed into two labels λ and s which are quantum numbers for the relative and center-of-mass motion, respectively. We assume that the total exciton wave function is a product of a wave function for the center-of-mass motion $\psi_s(\vec{r})$ and a wave function for the relative motion. At this point Eq. (15) still includes the possibility of spatial dispersion, which is discussed more fully in the Appendix.

Now we specialize to the case of no spatial dispersion, which means in particular neglect of the dependence of the exciton frequency $\omega_i\equiv\omega_{\lambda,s}$ upon the center-of-mass quantum number s, and also neglect of s dependence in any matrix elements. This will permit us to evaluate the sums over $i\equiv(\lambda,s)$ in Eq. (15) and so obtain simplified expressions.

In the case of an infinite crystal s stands for the momentum $\vec{k}$, $\psi_s(\vec{r})$ is simply a plane wave and the coupling function has the well known form

$$g_{\lambda\vec{k},\vec{k}'\gamma'}=g^{\gamma'}_{\lambda}\delta_{k,k'}\ .\tag{16}$$

In the case of a bounded medium, the coupling function $g_{\lambda s,\vec{k}'}$ can be calculated by expanding $\psi_s(\vec{r})$ in plane waves and using Eq. (16). The result is

$$g_{\lambda s,\vec{k}'\gamma'}=g^{\gamma'}_{\lambda}\psi_s(\vec{k})\ ,\tag{17}$$

where $\psi_s(\vec{k})$ is the Fourier transform of $\psi_s(\vec{r})$. Using the f sum rule

$$\omega_p^2=\frac{8\pi}{\hbar}\sum_{\lambda}|g^{\gamma'}_{\lambda}|^2\tag{18}$$

which permits us to eliminate ω_p^2 in the left-hand side of Eq. (15). Next we use the completeness of the set of $\psi_s(\vec{r})$ which states

$$\sum_s\psi_s^*(\vec{r})\psi_s(\vec{r}')=\begin{cases}\delta(\vec{r}-\vec{r}'),\\ \text{if both arguments}\\ \text{are in the crystal region;}\\ 0,\ \text{otherwise.}\end{cases}\tag{19}$$

Then the Fourier transform of Eq. (15) can be written

$$(-\omega^2-c^2\nabla^2)A_{\gamma}(\gamma)=4\pi\omega^2\int d\vec{r}\,\chi(\vec{r},\vec{r}')A_{\gamma}(\vec{r}')\tag{20}$$

which is Maxwell's equation for $\vec{A}(\vec{r})$ in a medium with

$$\chi(\vec{r},\vec{r}')=\begin{cases}\delta(\vec{r}-\vec{r}')\dfrac{2}{\hbar}\displaystyle\sum_{\lambda}\frac{|g^{\gamma}_{\lambda}|^2}{\omega_{\lambda}^2-(\omega\pm i\eta)^2},\\ \text{if both arguments are in}\\ \text{the crystal region;}\\ 0,\ \text{otherwise.}\end{cases}\tag{21}$$

It is clear from Eqs. (20) and (21) that in this case the integro-differential equation (20) is just a differential equation since the kernel as the right-hand side of Eq. (20) is local. The inhomogeneous equation (20) needs to be solved subject

to specifying asymptotic conditions on the homogeneous equation (right-hand side zero), which physically corresponds to vanishing exciton-photon coupling coefficient, i.e., $g_\lambda^\gamma = 0$. For this reason we put $\pm i\eta$ in the denominator in Eq. (21), with η a real positive infinitesimal quantity. The positive sign (negative sign) in front of $i\eta$ corresponds to "out" ("in") boundary conditions. The polariton operators $\hat{B}^\dagger_{\vec{k}_0\gamma}$ and $\hat{B}_{\vec{k}_0\gamma}$ can correspondingly be labeled with "in" and "out" to regulate the asymptotic photon solutions as either incoming or outgoing.

Summarizing, we have solved Maxwell's equation (20) with susceptibility equation (21) via diagonalizing H^{Pol}. Once $A(\vec{r})$ is known the other amplitudes can be determined from Eqs. (11)–(14). Equation (13) gives, in particular,

$$\alpha_\lambda(\vec{r}) = \frac{2i}{\omega}\left(\frac{2\pi}{\hbar}\right)^{1/2} \sum_\gamma \frac{\omega_\lambda^2 g_\lambda^\gamma}{\omega_\lambda^2 - (\omega \pm i\eta)^2} A_\gamma(\vec{r}), \quad (22)$$

if $\vec{r}$ is in the crystal region and 0 otherwise.

We can now discuss the physical significance of the states created by the $\hat{B}$ operators of Eq. (9). The photonlike part satisfies Maxwell's equation (20). The homogeneous solution of Eq. (20) is taken as an incoming or outgoing plane wave with wave vector $\vec{k}_0$ depending on whether we take $\pm i\eta$ in Eq. (21). The coupled solution of Eq. (20) will also contain reflected and transmitted waves outside the crystal as well as propagating polarization waves in the crystal. The interior and exterior parts are connected by the usual Maxwell boundary conditions. The exciton part of the state created by $\hat{B}^\dagger$ is obtained by solving Eq. (22) choosing $\pm i\eta$ as in Eq. (21). A state created by $\hat{B}^\dagger$ can be uniquely labeled by the momentum $\vec{k}_0$ of the exterior photon plus the "in" or "out" designation of an asymptotic behavior. In Sec. IV this will be illustrated for normal incidence on a semi-infinite crystal. Thus, as indicated at the beginning of this subsection the polariton operators may be denoted

$$\hat{B}^{\dagger\,\mathrm{out}}_{\vec{k}_0\gamma}, \quad \hat{B}^{\dagger\,\mathrm{in}}_{\vec{k}_0\gamma},$$

depending on choice of $\pm i\eta$ and their adjoints

$$\hat{B}^{\mathrm{out}}_{\vec{k}_0\gamma} \text{ and } \hat{B}^{\mathrm{in}}_{\vec{k}_0\gamma},$$

and when applied to the vacuum these create the appropriate states as indicated above. In what follows use will be made of this set of operators.

B. Exciton-phonon coupling

The exciton-phonon interaction for an infinite crystal can be written in the form

$$H' = \sum_{\substack{\vec{k},\vec{q}\\ \lambda,\lambda'}} f_{\lambda\lambda'}(\vec{q})\hat{b}^\dagger_{\lambda\vec{k}}\hat{b}_{\lambda',\vec{k}+\vec{q}}\hat{c}^\dagger_{\vec{q}} + \text{c.c.} \quad (23)$$

It was shown in Ref. 9 that for small momentum transfer $\vec{q}$ only two essentially different functions can arise:

$$f_{\lambda\lambda'}(\vec{q}) = \delta_{\lambda\lambda'}\left(\frac{r_0^3}{V}\right)^{1/2}(C_{cc'}\delta_{vv'} - C_{vv'}\delta_{cc'}), \quad (24)$$

$$f_{\lambda\lambda'}(\vec{q}) = \delta_{vv'}\delta_{cc'}\frac{C}{|\vec{q}|}\left(\frac{r_0^3}{V}\right)^{1/2} \times\left[F^{\lambda\lambda'}\left(\frac{m_e}{m_e+m_h}\vec{q}\right) - F^{\lambda\lambda'}\left(\frac{m_h}{m_e+m_h}\vec{q}\right)\right]. \quad (25)$$

Equation (24) corresponds to deformation potential and interband Fröhlich (that is either $v \neq v'$ or $c \neq c'$) scattering. Equation (25) describes intraband Fröhlich scattering. r_0 is the 1s-exciton radius and $F^{\lambda\lambda'}$ is given by

$$F^{\lambda\lambda'}(\vec{q}) = \int d\vec{r}\, e^{i\vec{q}\cdot\vec{r}}\varphi^*_\lambda(\vec{r})\varphi_{\lambda'}(\vec{r}). \quad (26)$$

$\varphi_\lambda(\vec{r})$ is the hydrogenic wave function with quantum label λ. The coupling equation (25) is linear in $\vec{q}$ for small $|\vec{q}|$ and therefore often called forbidden. Equation (23) reads, in r space,

$$H' = \sum_{\substack{\vec{q}\\ \lambda\lambda'}} f_{\lambda\lambda'}(\vec{q})\int d\vec{r}\,\hat{b}^\dagger_\lambda(\vec{r})\hat{b}_{\lambda'}(\vec{r}) \times e^{-i\vec{q}\cdot\vec{r}}\hat{c}^\dagger_{\vec{q}} + \text{c.c.} \quad (27)$$

This form for the exciton-phonon interaction can also be used for a finite crystal. The range of the $\vec{r}$ integration is then automatically only the crystal region.

III. DERIVATION OF THE SCATTERING EFFICIENCY

The differential cross section per unit volume, per unit scattered frequency interval for scattering of a photon with wave vector $\vec{k}_0$ into a photon with wave vector $\vec{k}_0'$ exciting a phonon $\vec{q}$ in the crystal is[20]

$$\frac{d^2\sigma}{d\Omega\, d\omega'} = \left(\frac{k_0'}{2\pi\hbar c}\right)^2 \sum_{\vec{q}} \delta[\omega - \omega' - \Omega(\vec{q})] \times |T_{\vec{k}_0'\gamma',\vec{q},\vec{k}_0\gamma}(\omega + i\eta)|^2, \quad (28)$$

with

$$T_{\vec{k}_0'\gamma',\vec{q},\vec{k}_0\gamma}(\omega + i\eta) = \langle\tilde{0}|\hat{a}_{\vec{k}_0'\gamma'}\hat{c}_{\vec{q}} \times T^{H^{\mathrm{PE}},H'}(\omega + i\eta)\hat{a}^\dagger_{\vec{k}_0\gamma}|\tilde{0}\rangle. \quad (29)$$

H^{PE} is the photon-exciton interaction in the polariton Hamiltonian (3) and $|\tilde{0}\rangle$ is the product of the free photon, exciton, and phonon vacuum states. The T operator is

$$T^{H^{PE},H'}(\omega+i\eta) = (H^{PE}+H') + (H^{PE}+H')\frac{1}{\hbar(\omega+i\eta)-H}(H^{PE}+H') . \tag{30}$$

The T operator in Eq. (30) describes the scattering of photons by two potentials H^{PE} and H'. The theory of scattering of a particle by two potentials has been discussed in Ref. 21 and we shall take over that discussion making necessary modifications. Our first step is to write Eq. (30) using an operator identity which can be established after some algebra

$$T^{H^{PE},H'}(z) = H^{PE}\frac{1}{z-H+H'}(z-H+H'+H^{PE}) + \left(1+H^{PE}\frac{1}{z-H+H'}\right)T^{H'}(z) \times \left(1+\frac{1}{z-H+H'}H^{PE}\right). \tag{31}$$

Since the first term in Eq. (31) is independent of the exciton-phonon interaction it does not contribute to the inelastic scattering and we therefore omit it in the following.

The operator in parentheses in the second term when applied as in Eq. (29) will permit us to introduce new states. The application of this operator to the ket $a^{\dagger}_{\vec{k}_0}|\tilde{0}\rangle$ will produce a new state which we call $|\phi^{\vec{k}_0}\rangle$, which can be labeled by the "in" and "out" labels. This state can be identified as an eigenstate of H^{Pol}. Thus let the new states be[22]

$$|\phi^{out}_{\vec{k}_0\gamma}\rangle = \left(1+\frac{1}{\hbar(\omega+i\eta)-H^{Pol}}H^{PE}\right)\hat{a}^{\dagger}_{\vec{k}_0\gamma}|\tilde{0}\rangle ,$$
$$|\phi^{in}_{\vec{k}_0\gamma}\rangle = \left(1+\frac{1}{\hbar(\omega-i\eta)-H^{Pol}}H^{PE}\right)\hat{a}^{\dagger}_{\vec{k}_0\gamma}|\tilde{0}\rangle . \tag{32}$$

For vanishing exciton-photon coupling equation (32) reduces to a photon plane wave. Choosing the plus (+) or minus (−) sign with $(i\eta)$ in Eq. (32) produces "out" or "in" going scattered waves. The state equation (32) is an eigenstate of H^{Pol}, using a general theorem in formal scattering theory.[22]

Now recall the definition of the $\hat{B}^{\dagger}_{\vec{k}_0\gamma}$ operator in Eq. (9), and its amplitudes A and α in Eqs. (20) and (22). For vanishing exciton-photon coupling $\alpha=0$ and the $\hat{B}^{\dagger}_{\vec{k}_0\gamma}$ operator reduces to $\hat{A}_{\vec{k}_0\gamma}$. As discussed in the end of Sec. IIA, depending on choice of $\pm i\eta$ in Eqs. (21) and (22), these operators become the $B^{\dagger\,out}_{\vec{k}_0\gamma}$ and correspondingly the "in" operators which describe "out" and "in" scattered waves.

However a solution of the Schrödinger equation which describes scattering of a particle in a potential is uniquely determined by the incident wave vector of the particle (here photon) and the asymptotic behavior. Thus (apart from possibly a phase factor), we identify

$$|\phi^{out}_{\vec{k}_0\gamma}\rangle \equiv \hat{B}^{\dagger\,out}_{\vec{k}_0\gamma}|0\rangle \tag{33a}$$

and

$$|\phi^{in}_{\vec{k}_0\gamma}\rangle \equiv \hat{B}^{\dagger\,in}_{\vec{k}_0\gamma}|0\rangle . \tag{33b}$$

This important step permits us to rewrite the original transition matrix element between bare photon states as a matrix element between appropriate polariton states. Then Eq. (29) becomes[21]

$$T_{\vec{k}_0'\gamma',\vec{q},\vec{k}_0\gamma} = \langle 0|\hat{B}^{in}_{\vec{k}_0'\gamma'}\hat{c}_{\vec{q}}H'\hat{B}^{\dagger\,out}_{\vec{k}_0\gamma}|0\rangle$$
$$= \sum_{ij} f_{ij}(\vec{q})\langle 0|\hat{B}^{in}_{\vec{k}_0'\gamma'}\hat{b}^{\dagger}_i\hat{b}_j\hat{B}^{\dagger\,out}_{\vec{k}_0\gamma}|0\rangle$$
$$= \sum_{ij} f_{ij}(\vec{q})\{\langle 0|[\hat{B}^{in}_{\vec{k}_0'\gamma'},\hat{b}^{\dagger}_i][\hat{b}_j,\hat{B}^{\dagger\,out}_{\vec{k}_0\gamma}]+[\hat{B}^{in}_{\vec{k}_0'\gamma'},\hat{b}_j][\hat{b}^{\dagger}_i,\hat{B}^{\dagger\,out}_{\vec{k}_0\gamma}]|0\rangle\},$$

and using Eq. (22) this becomes

$$T_{\vec{k}_0'\gamma',\vec{q},\vec{k}_0\gamma} = \sum_{ij}(\alpha_i^{\vec{k}_0'\gamma'})^{*\,in}(\alpha_j^{\vec{k}_0\gamma})^{out}\frac{f_{ij}(\vec{q})(\omega_i+\omega')(\omega_j+\omega)+f_{ji}(\vec{q})(\omega-\omega_j)(\omega'-\omega_i)}{\omega_i^{3/2}\omega_j^{3/2}} . \tag{34}$$

If we transform the $\vec{k}$ label in $i=(\lambda,\vec{k})$ into $\vec{r}$ space and use Eq. (27), Eq. (34) reads

$$T_{\vec{k}_0'\gamma',\vec{q},\vec{k}_0\gamma} = 2\sum_{\lambda\lambda'}\frac{f_{\lambda\lambda'}(\vec{q})(\omega_\lambda\omega_{\lambda'}+\omega\omega')}{\omega_\lambda^{3/2}\omega_{\lambda'}^{3/2}}\int d\vec{r}\, e^{-i\vec{q}\cdot\vec{r}}[\alpha_{\lambda'}^{\vec{k}_0'\gamma'}(\vec{r})]^{*\,in}[\alpha_{\lambda}^{\vec{k}_0\gamma}(\vec{r})]^{out} . \tag{35}$$

Inserting Eqs. (22) and (35) into Eq. (28) and rearranging, gives

$$\frac{d^2\sigma}{d\Omega\, d\omega'} = k_0 k_0'^3 \sum_{\vec{q}} \delta[\omega - \omega' - \Omega(\vec{q})] \left| \sum_{\gamma\gamma'} R_{\gamma\gamma'}(\vec{q},\omega) S_{\gamma\gamma'}(\vec{q}) \right|^2 , \tag{36}$$

$$R_{\gamma\gamma'}(\vec{q},\omega) = \sum_{\lambda\lambda'} \frac{\omega_\lambda^{1/2} g_\lambda^\gamma f_{\lambda\lambda'}(\vec{q}) g_{\lambda'}^{\gamma'*} \omega_{\lambda'}^{1/2}}{\omega\omega'} \times \left(\frac{1}{[\hbar\omega_\lambda - \hbar(\omega + i\eta)][\hbar\omega_{\lambda'} - \hbar(\omega' + i\eta)]} + \frac{1}{[\hbar\omega_\lambda + \hbar(\omega + i\eta)][\hbar\omega_{\lambda'} + \hbar(\omega' + i\eta)]} \right) , \tag{37}$$

$$S_{\gamma\gamma'}(\vec{q}) = \int_C d\vec{r}\, e^{-i\vec{q}\cdot\vec{r}} A^{\vec{k}_0'\gamma',\text{in}*}(\vec{r}) A^{\vec{k}_0\gamma,\text{out}}(\vec{r}) . \tag{38}$$

The vector potential A in Eq. (38) is determined by Maxwell's equation (20) and the condition that outside the crystal the incident or scattered wave $\vec{k}$ taken to be unit amplitude. The prefactor in Eq. (36) is calculated using this boundary condition. The letter C in Eq. (38) means that the r integral runs only over the crystal. Without damping ($d^2\sigma/d\Omega\, d\omega'$) is proportional to the crystal volume, and with damping it is proportional to an effective scattering volume. One obtains the scattering efficiency {dimension[1/(length times frequency)]} from the cross section $d^2\sigma/d\Omega\, d\omega'$ [dimension (length squared/frequency)] by calculating the latter for unit volume.

IV. DISCUSSION OF THE SCATTERING CROSS SECTION

A major result of this work is Eq. (36) for the scattering cross section, which consists of two factors: the Raman tensor $R(\vec{q},\omega)$ and a structure factor $S(\vec{q})$. This result was obtained by neglect of spatial dispersion. Now we shall compare Eq. (36) with the results of perturbation theory and with other (conventional) treatments in the polariton picture.

In the perturbation theory treatment the structure of the Hamiltonian is identical to that of Eq. (2) except that all objects always refer to the infinite crystal (interior), in the calculated $(\partial^2\sigma/\partial\Omega\,\partial\omega')_I$, with the transmission factors across the boundaries being accounted for as in Eq. (1). A comparison of our equation (37) with the results of perturbation theory [see Eqs. (29) and (30) of Ref. 2] indicates first of all that Eq. (37) only contains two of the six terms which arise in perturbation-theory treatments.[2] This is because of the simplicity of the Hamiltonian we used: had we included the bilinear exciton-phonon and the trilinear exciton-photon terms the other four terms would appear in Eq. (37). But the result equation (37) suffices for our discussion. Further, we note that the two terms in Eq. (37) are the same as their counterparts with one important difference. In our case $\vec{q}$ is the difference between incident and scattered polariton momenta inside the crystal whereas in perturbation theory, $\vec{q}$ is the difference between incident and scattered bare-photon momenta. In case of momentum independent scattering (such as deformation potential or interband Frohlich coupling), the two results agree. For the intraband Frohlich case, $R(\vec{q},\omega)$ is proportional to the momentum transfer $\vec{q}$ and thus in polariton theory $\vec{q} = [n(\omega)\vec{k}_0 - n(\omega')\vec{k}_0']$, where $n(\omega)$ is the refractive index, while in perturbation theory $\vec{q} = (\vec{k}_0 - \vec{k}_0')$. As ω approaches a discrete exciton energy from below the polariton momentum transfer can become very large whereas the photon momentum transfer remains small.

The structure factor S in Eq. (38), in general, leads to Loudon's formula[1] for transmission coefficients, absorption corrections, etc. To illustrate this let us consider a backward-scattering experiment with normal incidence on a semi-infinite crystal. The different amplitudes for the vector potential which are compatible with the boundary conditions "in" and "out" are shown in Fig. 1(a) for the incident wave and in Fig. 1(b) for the scattered wave. Figure 1(a) is apparent because it corresponds to a simple physical picture for the

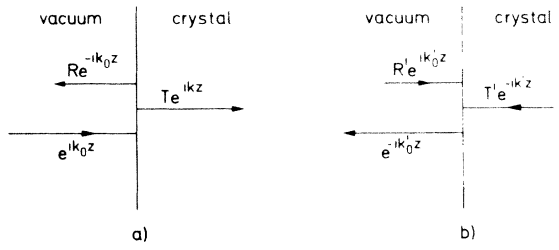

FIG. 1. Illustration of the different waves inside and outside of the crystal which belong to the initial and final state for the Raman scattering and which satisfy the correct boundary conditions. (a) Incident wave; (b) scattered wave.

incoming, reflected and transmitted waves. Figure 1(b) for the scattered waves is at first sight unexpected. However, examining Eq. (32) reveals the origin of this result: one has to change the bra vector [Eq. (32)] into a ket vector by taking the Hermitian adjoint. This changes the sign of $i\eta$ into $-i\eta$ and therefore the ket of the scattered waves corresponds to incoming boundary conditions. A discussion of this point in terms of precollision and postcollision wave packets is given in Ref. 21. Maxwell's equation (20) gives, for the amplitudes,

$$1+R=T, \quad 1-R=nT, \tag{39}$$

with $n=k/k_0$ and $n^2=\epsilon(\omega)$. It then follows that $T=2/(1+n)$. Similarly, Fig. 1(b) leads to $T'=2/(1+n')$. Therefore, we have the result that the same transmission coefficients have to be used for the incident and scattered waves, except for the difference between ω and ω'.

Equation (38) then becomes, after squaring,

$$|S(q_z)|^2 = F^2[\mathrm{Re}^2(k'-k+q_z)+\mathrm{Im}^2(k'+k)]^{-1} \times T(\omega)T(\omega') . \tag{40}$$

$|S(q_z)|^2$ acts like a smeared out momentum selection rule for the final q_z integration. The main contribution comes from a region around $q_z = \mathrm{Re}(k-k')$ with a width of $\mathrm{Im}(k+k')$. Since the deformation potential is $\vec{q}$ independent there should be no effect at all in the cross section for allowed scattering. But Frohlich scattering is $\vec{q}$ dependent and one would expect an effect. The magnitude of this effect can be estimated in the following way: the maximum in the Frohlich coupling for $1s$ excitons occurs at $|\vec{q}| \approx 1/r_0$, where r_0 is the $1s$-exciton radius. The spread of momentum is of the order $\mathrm{Im}(k+k') \sim k_0$. Because k_0 is small compared to $1/r_0$ the spread involves only a region in $\vec{q}$ space, small compared to $(1/r_0)^3$ and therefore should lead to a small effect. This was verified by a numerical calculation for CdS which showed that to obtain non-negligible effects one would need an imaginary refractive index much larger than one.

Carrying out the q_z integration one obtains from the $|S|^2$ term

$$T(\omega)T(\omega')F/\mathrm{Im}(k+k'), \tag{41}$$

except for a volume factor which is canceled by a similar factor in R.

Equation (36) together with Eq. (41) give a final answer to the question of which $(d^2\sigma/d\Omega\,\sigma\omega')_I$ has to be used in equations like (1). We have treated the exciton-photon interaction exactly in this work, so it is clearly a *polariton* picture. Nevertheless, we obtain a result for $(\partial^2\sigma/\partial\Omega\,\partial\omega')$ which is formally equal to the lowest-order perturbation result with the exception that the transferred momentum in the Raman tensor refers to polariton momenta inside the crystal before and after scattering and not to bare-photon momenta. As a result the correct $(\partial^2\sigma/\partial\Omega\,\partial\omega')_I$ is formally identical to the lowest-order perturbation theory result with the previously indicated difference depending on whether the scattering is momentum independent or momentum dependent (intraband Frohlich). Now we shall compare our result equation (36) with the cross sections obtained in other polariton picture treatments such as Refs. 3, 5, 7, and 9. In Refs. 3 and 5, a result is obtained which, transcribing to our notation can be written, for unit volume ($V=1$),

$$\frac{d^2\sigma}{d\Omega\,d\omega'} = \frac{1}{4\pi^2\hbar^2}\frac{1}{v}\frac{k'^2}{v'}\sum_{\vec{q}}\delta(\omega-\omega'-\Omega(\vec{q}))\Delta_{\vec{q},\vec{k}-\vec{k}'} \times\left|\sum_{\substack{\lambda,\lambda'\\ \gamma,\gamma'}}\vec{\epsilon}_\gamma E_\lambda^\gamma(\omega) f_{\lambda\lambda'}(\vec{q})\frac{16\pi}{\hbar} \times\left(1+\frac{\omega_\lambda\omega_{\lambda'}}{\omega\omega'}\right)E_{\lambda'}^{\gamma'*}(\omega')\vec{\epsilon}'_{\gamma'}\right|^2 . \tag{42}$$

v is the group velocity (Ref. 3 uses the energy transport velocity) of the incident polariton. v' is the group velocity and $\vec{k}'$ is the wave vector of the scattered polariton. The factor k'^2/v' is proportional to the density of final polariton states. Δ is the Kronecker symbol and $\vec{\epsilon}$ and $\vec{\epsilon}'$ the polarization of the polaritons. The quantity $E_\lambda^\gamma(\omega)$ measures the exciton content of the polariton and is given by

$$E_\lambda^\gamma(\omega) = \frac{g_\lambda^\gamma\omega_\lambda^{1/2}}{\omega_\lambda^2-(\omega+i\eta)^2}\frac{(\omega)^{1/2}}{2}N(\omega),$$
$$N(\omega) = \left(1+\frac{8\pi}{\hbar}\sum_\lambda\frac{g_\lambda^{\gamma 2}\omega_\lambda^2}{(\omega_\lambda^2-\omega^2)^2}\right)^{-1/2} . \tag{43}$$

Equation (42) should be compared with our equation (36) taking

$$S(\vec{q}) \approx \Delta_{\vec{q},\vec{k}-\vec{k}'} . \tag{44}$$

There are two important differences between our result equation (36) and equation (42).

In our result equation (36), the velocity factor in the incident flux, and the density of final states refers to the propagation of the physical (measured) photons outside the crystal, while in Eq. (42) these refer to the propagation of polariton wave packets (for group or energy velocity) inside the crystal. We believe our result resolves the question (and difficulties) referred to earlier

of use of group or energy velocity, in the polariton picture, especially when absorption is present. From our treatment we see that the correct velocity factor is that of photons in vacuum.

The second difference concerns the normalization constant $N(\omega)$. In our treatment, e.g., Eq. (37), $N(\omega)=1$ and the correct normalization factors are determined by the Maxwell boundary conditions (recall spatial dispersion is not included here so there are no *abc*). These factors then appear in the transmission coefficients. Again we stress that our cross section corresponds to the physical situation where the incident and scattered photons are measured outside the crystal and the scattering by phonons is done by polaritons inside the crystal. On the other hand, the normalization constant $N(\omega)$ in Eq. (43) corresponds to normalized polaritons. Thus Eqs. (42) and (43) describe the situation in which incident and scattered polariton fluxes are presumed created (normalized) and detected inside the crystal. But in our opinion the latter does not correspond to the physical situation. For this reason also we believe our treatment preferable.

At resonance, when incident (or scattered) frequency approaches a dispersionless 1*s* exciton band our treatment equation (36) leads to a divergence in the scattering cross section like $(\omega_{1s}-\omega)^{-2}$. Of course it is well known that any predicted divergence is eliminated just at resonance by damping (self-energy effects) which are due to higher-order terms in the Hamiltonian than we considered. But we want to emphasize that this unphysical divergence is not a significant defect of the theory but only of the somewhat simplifying approximations we made here with the assumed Hamiltonian in order to bring out the important new results of our work. Inclusion of spatial dispersion effects (see Appendix) even if damping terms are neglected also eliminates the divergence. But spatial dispersion effects complicate the theory owing to the extra propagating waves,[23] etc., so that a straightforward comparison of our new results and other polariton treatments including spatial dispersion is not possible. Our predicted divergence is in accord with the results of perturbation theory carried out at a similar level. As will be shown (Secs. 5 and 6) explicit numerical calculations of the frequency dependent cross section near resonance using our results give satisfactory agreement with experiment in several cases, although several questions remain. Turning now to the conventional polariton treatments we note that Ref. 6 obtains the result equation (42) with $N=1$. In Ref. 9, a formula like Eq. (36) is obtained, but multiplied by the factor $\mathrm{Re}(n')/\mathrm{Re}(n)$. All these other polariton treatments, Refs. 3, 5, 6, 7, and 9 obtain a cross section which diverges at resonance like $(\omega_{1s}-\omega)^{-3/2}$, again neglecting damping and spatial dispersion, and with the same caveat regarding elimination of unphysical divergences at resonance, by damping terms.

We do not know whether at the present time the predicted difference between the power law divergence of (-2) we predict or that of $(-\frac{3}{2})$ given by other theories, is experimentally detectable, but certainly this is a noteworthy difference between our new results (and perturbation theory) and the other polariton theories.

V. EVALUATION OF THE RAMAN TENSOR

In the present section we shall derive more explicit formulas for the resonant term in the Raman tensor equation (37). In Sec. VI explicit numerical calculations will be given and compared with experiment in various cases. Owing to our general result that the rigorous polariton treatment gives results akin to perturbation theory there will be some contact with results previously reported by other workers. Where such contact exists we compare our work and theirs. We believe that the several of the various representations for the Raman tensor and the structure factor reported here are new and also permit numerical calculation to greater accuracy than before.

We consider a simple insulator and we limit ourselves to one valence and one conduction band and the corresponding discrete and continuous exciton states. The bands are assumed to be parabolic and the band masses negative and positive for the valence and conduction band, respectively. The quantum number λ is then fully determined by the internal exciton momentum $\vec{k}$ and (only for the Wannier exciton case) a discrete variable $n=1, 2, 3\ldots$. The oscillator strength g_λ^γ is[24]

$$g_\lambda^\gamma=(e/m)\langle p_\gamma\rangle(\omega_\lambda)^{-1/2}\psi_\lambda(0),$$
$$\langle p_\gamma\rangle=\int d\vec{r}\,\varphi_v^*(\vec{r})p_\gamma\varphi_c(\vec{r}), \tag{45}$$

where φ is a Bloch function at the zone center. The momentum matrix element is assumed to be nonzero. For free electron-hole pairs

$$|\psi_{\vec{k}}(0)|^2=1, \tag{46}$$

while for Coulomb correlated pairs

$$|\psi_n(0)|^2=\frac{1}{\pi r_0^3 n^3},\quad |\psi_{\vec{k}}(0)|^2=\frac{\pi}{r_0|\vec{k}|}\,\frac{e^{\pi/r_0|\vec{k}|}}{\sinh(\pi/r_0|\vec{k}|)}, \tag{47}$$

where r_0 is the 1*s* exciton radius.

A. Allowed scattering

The coupling function is given by Eq. (24) and the Raman tensor for correlated electron-hole pairs becomes

$$R_{\gamma\gamma'}(\omega)=\left(\frac{r_0}{V}\right)^{1/2}\frac{e^2\langle p_\gamma\rangle\langle p_{\gamma'}\rangle^*(C_{cc}-C_{vv})}{\omega\omega' m^2}\left(\sum_n \frac{1}{\pi r_0^3 n^3}\,\frac{1}{[\hbar(\omega+i\eta)+E_B/n^2-E_g][\hbar(\omega'+i\eta)+E_B/n^2-E_g]}\right.$$
$$\left.+\frac{1}{2\pi r_0}\int_0^\infty dk\,k\,\frac{e^{\pi/r_0|\vec{k}|}/\sinh(\pi/r_0|\vec{k}|)}{[\hbar(\omega+i\eta)-\hbar^2k^2/2\mu-E_g][\hbar(\omega'+i\eta)-\hbar^2k^2/2\mu-E_g]}\right). \tag{48}$$

E_B is the exciton binding energy $\hbar^2/2\mu r_0^2$ of the 1s exciton, μ is the reduced mass. Writing the numerator in the more symmetric way

$$e^{\pi/r_0|\vec{k}|}/\sinh(\pi/r_0|\vec{k}|)=1+\coth(\pi/r_0|\vec{k}|)$$

and making the substitution $x=1/kr_0$ the integration can be carried out in the complex plane. The integration path is hereby extended for convenience to $-\infty$ and then closed in the upper plane. The result is

$$R_{\gamma\gamma'}(\omega)=\left(\frac{r_0}{V}\right)^{1/2}\frac{e^2\langle p_\gamma\rangle\langle p_{\gamma'}\rangle^*(C_{cc}-C_{vv})}{4\pi r_0^3\omega\omega' m^2}\left[\sum_{n=1}^{\infty}\frac{1}{n^3}\,\frac{1}{\hbar(\omega+i\eta)-E_g+E_B/n^2}\,\frac{1}{\hbar(\omega'+i\eta)-E_g+E_B/n^2}\right.$$
$$+\frac{1}{\hbar\omega_0 E_B}\left(\ln\left|\frac{\hbar(\omega+i\eta)-E_g}{\hbar(\omega'+i\eta)-E_g}\right|\right.$$
$$+i\pi\{\Theta[(\hbar\omega-E_g)/\hbar\omega_0]-\Theta[(\hbar\omega'-E_g)/\hbar\omega_0]\}$$
$$\left.\left.+i\pi(\coth\{\pi[E_B/(\hbar\omega-E_g)]^{1/2}-\coth\{\pi[E_B/(\hbar\omega'-E_g)]^{1/2}\right)\right]. \tag{49}$$

Here $\Theta(x)$ denotes the step function. The case of uncorrelated pairs is obtained from Eq. (49) by taking the limit $r_0\to\infty$,

$$R_{\gamma\gamma'}(\omega)=i\left(\frac{r_0}{V}\right)^{1/2}\frac{e^2\langle p_\gamma\rangle\langle p_{\gamma'}\rangle^*(C_{cc}-C_{vv})}{4\pi\omega\omega'(\hbar\omega_0)^{1/2}m^2}\left(\frac{2\mu}{\hbar^2}\right)^{3/2}\left[\left(\frac{\hbar\omega-E_g}{\hbar\omega_0}\right)^{1/2}-\left(\frac{\hbar\omega'-E_g}{\hbar\omega_0}\right)^{1/2}\right]. \tag{50}$$

B. Forbidden scattering

In this case the coupling function equation (25) is to be used. It is convenient to write the intermediate sum as a Green's function

$$\mathcal{G}_{\omega+i\eta}(\vec{r}_1,\vec{r}_2)=\sum_\lambda \frac{\langle\vec{r}_1|\lambda\rangle\langle\lambda|\vec{r}_2\rangle}{\hbar(\omega+i\eta)-\hbar\omega_\lambda}. \tag{51}$$

Using Eq. (50) we obtain

$$R_{\gamma\gamma'}(\vec{q},\omega)=\left(\frac{r_0}{V}\right)^{1/2}\frac{\langle p_\gamma\rangle\langle p_{\gamma'}\rangle^* C}{r_0^4 E_B^2|\vec{q}|\omega\omega'}\,\frac{e^2}{m^2}$$
$$\times\left[S_\omega\left(\vec{q}\,\frac{m_e}{M}\right)-S_\omega\left(\vec{q}\,\frac{m_h}{M}\right)\right], \tag{52}$$

$$S_\omega(\vec{q})=(r_0^2E_B)^2\int d\vec{r}\,e^{i\vec{q}\cdot\vec{r}}$$
$$\times\mathcal{G}_{\omega+i\eta}(0,\vec{r})\mathcal{G}_{\omega'+i\eta}(\vec{r},0), \tag{53}$$

with the total exciton mass $M=m_e+m_h$. In the uncorrelated case it is

$$\mathcal{G}_{\omega+i\eta}(\vec{r},0)=\mathcal{G}_{\omega+i\eta}(0,\vec{r})=\frac{1}{r_0^2E_B}\,\frac{1}{4\pi|\vec{r}|}\,e^{ik|\vec{r}|}, \tag{54}$$

and in the Coulomb correlated case[25]

$$\mathcal{G}_{\omega+i\eta}(\vec{r},0)=\mathcal{G}_{\omega+i\eta}(0,\vec{r})=\frac{1}{r_0^2E_B}\,\frac{\Gamma(1-i\nu)}{4\pi|\vec{r}|}$$
$$\times W_{i\nu,1/2}(-2ik|\vec{r}|). \tag{55}$$

Γ is the gamma function, W is the Whittaker function, and k and ν are defined by

$$k=\left(\frac{\hbar(\omega+i\eta)-E_g}{E_B}\right)^{1/2},\quad \mathrm{Im}(k)>0, \tag{56}$$

$$\nu=1/r_0k. \tag{57}$$

Inserting Eq. (54) in (53) gives for the uncorrelated case

$$S_\omega(\vec{q}) = \frac{1}{4\pi|\vec{q}|} \arctan \left\{ iqr_0 \left(\frac{E_B}{\hbar\omega_0}\right)^{1/2} \left[\left(\frac{\hbar\omega - E_g}{\hbar\omega_0}\right)^{1/2} - \left(\frac{\hbar\omega' - E_g}{\hbar\omega_0}\right)^{1/2}\right]\right\}. \quad (58)$$

Retaining only the term proportional to q^2, Eq.(52) yields the following expression for the Raman tensor for free electron-hole pairs:

$$R_{\gamma\gamma'}(\vec{q},\omega) = iq^2 \left(\frac{r_0}{V}\right)^{1/2} \frac{e^2\langle p_\gamma\rangle\langle p_{\gamma'}\rangle^* C}{12\pi\omega\omega' m^2} \frac{m_e - m_h}{M} \frac{1}{(\hbar\omega_0)^{3/2}} \left(\frac{2\mu}{\hbar^2}\right)^{1/2} \left[\left(\frac{\hbar\omega - E_g}{\hbar\omega_0}\right) - \left(\frac{\hbar\omega' - E_g}{\hbar\omega_0}\right)^{1/2}\right]^3. \quad (59)$$

The case of Coulomb correlated pairs is more tedious. We used the following spectral representation for the Whittaker function[26]:

$$W_{k,1/2}(x) = \frac{1}{\Gamma(1-k)} \frac{x}{2} \int_1^\infty ds\, e^{-xs/2} \left(\frac{s+1}{s-1}\right)^k, \quad (60)$$

which is valid for $-1 < \mathrm{Re}(k) < 1$. The last restriction means that the frequencies ω or ω' must be below the $1s$ exciton or above the gap:

$$\hbar\omega < E_{1s} \text{ or } \hbar\omega > E_g$$

and (61)

$$\hbar\omega' < E_{1s} \text{ or } \hbar\omega' > E_g .$$

Inserting Eqs. (55) and (60) into (53) and carrying out the $\vec{r}$ integration, we obtain

$$S_\omega(\vec{q}) = \frac{kk'}{2\pi} \int_1^\infty ds_1 \int_1^\infty ds_2 \frac{i\beta}{(q^2-\beta^2)^2} \times \left(\frac{s_1+1}{s_1-1}\right)^{i\nu} \left(\frac{s_2+1}{s_2-1}\right)^{i\nu'}, \quad (62)$$

with $\beta = ks_1 + k's_2$. For first-order Raman scattering, $q \ll \beta$ holds for all frequencies. We expand therefore the first factor in the integrand and keep only the quadratic term in $\vec{q}$ [the constant term in $\vec{q}$ drops out in Eq. (52)]. $S_\omega(\vec{q})$ then becomes[27]

$$S_\omega(\vec{q}) = \frac{2ikq^2}{\pi k'^4\alpha^5} B(1-i\nu', 4) \int_1^\infty ds_1 \left(\frac{s_1+1}{s_1-1}\right)^{i\nu} \times F(1-i\nu', 5, 5-i\nu', 1-2/\alpha). \quad (63)$$

Here $\alpha = 1 + (k'/k)s_1$, B is the β function, and F is the hypergeometric function. Moreover we assumed that ω' (and therefore also ω) is in the continuum so that $\alpha > 2$. The case $\hbar\omega < E_{1s}$ is easily obtained by interchanging k and k'. We expand the F function in Eq. (63) either as a power series in $1 - 2/\alpha$ (expansion I) or in $2/\alpha$ (expansion II) using the formulas 15.1.1 and 15.3.12 of Ref. 28. The substitution $s_1 \to s_1/(s_1+b)$ transforms the integral into the interval $[0,1]$. Finally, we expand also a factor of the form

$$\left(1 + \frac{k'-k}{2k} y\right)^{i\nu}, \quad 0 \le y \le 1$$

in a power series in y using the fact that $(k'-k)/2k \ll 1$. Our final expressions are

expansion I:

$$S_\omega(\vec{q}) = \frac{ik'q^2}{8\pi k^4\delta^5} B(1-i\nu', 4) \sum_{n=0}^\infty \frac{(5)_n (1-i\nu')_n}{(5-i\nu')_n} J_n, \quad (64)$$

$$J_n = \sum_{l_1=0}^\infty \sum_{l_2=0}^n \binom{n}{l_2} \binom{-5-n}{l_1} \times \left(\frac{1-\delta}{\delta}\right)^{n+l_1-l_2} B(4, 1+l_1+l_2-i\nu); \quad (65)$$

expansion II:

$$S_\omega(\vec{q}) = \frac{ik'q^2}{8\pi k^4\delta^4} \left(I_{-1}(\tfrac{1}{8}, 0) - i\nu' \sum_{n=0}^\infty \frac{(1-i\nu')_n (5)_n}{n!(1+n)!} 2^n \times I_n[\ln 2 - \psi(n+1) - \psi(n+2) + \psi(n+5) + \psi(1+n-i\nu'), 1] \right), \quad (66)$$

$$I_n(A,B) = \left(\frac{k'}{k}\right)^n \delta^{-n-i\nu} \times \sum_{l_1=0}^\infty \binom{i\nu}{l_1} (\delta-1)^{l_1} B(4+n, l_1+1-i\nu) \times \left[A + B\ln\left(\frac{2k\delta}{k'}\right) - B[\psi(n+4) - \psi(5+l_1+n-i\nu)\right]. \quad (67)$$

δ is given by $(k+k')/2k$ and ψ is the first psi function. Equations (64) and (65) represent a power series in $(1-\delta)/\delta$ and should converge rapidly far away from E_g and E_{1s}. Similarly, Eqs. (66) and (67) converge near E_g and E_{1s}.

Our numerical work using these formulas was carried out on the NYU-CDC-6600 computer. Detailed results are given in Sec. VI. It may be worth noting however that the numerical summation shows that the l_1 sum rapidly converges; taking 20 terms is sufficient for an accuracy of 10^{-7}.

For the n sums we used 300 summands in Eqs. (64) and 60 in Eq. (66). Taking both expansions, we obtained an estimated accuracy of at least 10^{-3} for all frequencies satisfying the inequalities in Eq. (61).

VI. DISCUSSION OF THE NUMERICAL RESULTS AND COMPARISON WITH EXPERIMENT

In this section we shall give our calculated results on the Raman tensor for the four combinations we considered: allowed and forbidden scattering, and Bloch and Wannier electronic states. As appropriate comparisons will be given with experiments in CdS and GaP and with other workers where there is some overlap.

Figures 2 and 3 show numerical results for the squared modulus of the Raman tensor $|R_{\gamma\gamma'}(\omega)|^2$ as function of the incident frequency ω. In both figures only an over-all numerical factor is arbitrary. The ratio of the values below and above the gap and also those for uncorrelated and correlated electron-hole pairs are fixed by the theory. We used the experimental value 0.75 for the ratio $E_B/\hbar\omega_0$ in CdS. For incident frequencies $\omega < \omega_{1s}$ our curves agree with those of Bendow *et al.*[17] for allowed scattering and of Martin[19] for forbidden scattering. Inspection of Eqs. (50) and (59) shows at once two important properties of the Raman tensor, calculated with free electron-hole pairs: (a) $|R_{\gamma\gamma'}(\omega)|^2$ as function of ω is symmetric with respect to the frequency $\Omega = \omega_g + \frac{1}{2}\omega_0$. The dashed lines in Figs. 2 and 3 show graphically this symmetry; (b) $R_{\gamma\gamma'}(\omega)$ is real for $\omega < \omega_g$ expressing the fact that only virtual electronic processes can take place in that frequency region. $R_{\gamma\gamma'}(\omega)$ is pure imaginary for $\omega > \omega_g + \omega_0$ and reflects the fact that the ingoing and outgoing photons are in resonance with electronic states. For $\omega_g < \omega < \omega_g + \omega_0$ $R_{\gamma\gamma'}(\omega)$ is in general complex. The dashed (real part) and dash-dotted (imaginary part) lines in Figs. 4 and 5, labeled with a capital F,

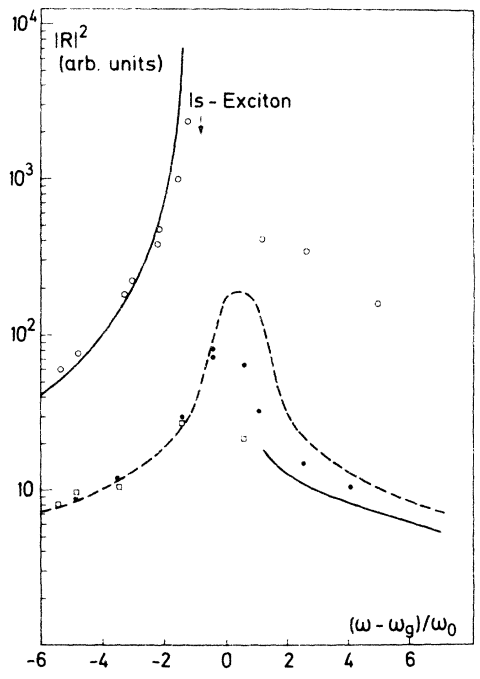

FIG. 2. Frequency dependence of the squared modulus of a nonzero component of the Raman tensor for allowed scattering. ω is the incident frequency; ω_g is the gap frequency. The dashed curve is calculated for free electron hole pairs and the solid curve is calculated for Wannier excitons. The arrow marks the position of the 1s exciton. The experimental points are from the following references: solid dots, Ref. 30 for GaP; open squares, Ref. 29 for GaP; open circles, Ref. 17 for CdS.

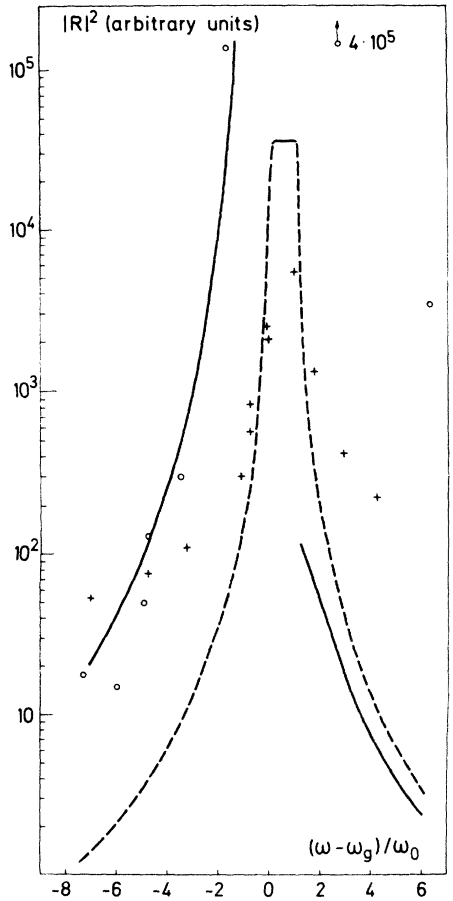

FIG. 3. Frequency dependence of the squared modulus of a nonzero component of the Raman tensor for forbidden scattering. Dashed curve calculated for free electron-hole pairs, solid curve calculated for Wannier excitons. The experimental points are from the following references: crosses, Ref. 30 for GaP; open circles, Ref. 31 for CdS.

illustrate these points.

The residual Coulomb attraction between electron and hole produces two changes compared to the free cases: discrete states appear below the gap and the oscillator strength [see Eqs. (50)–(52)] strongly increases for small kinetic energies of the exciton. Let us first consider allowed scattering. The discrete contribution to the Raman tensor is shown by the solid line in Fig. 4. Although the oscillator strength of the discrete states is much smaller than the integrated oscillator strength of the continuum, the discrete contribution is larger than the free electron-hole contribution in the region from $4\omega_0$ below to $3\omega_0$ above the gap. The strong $1/k$ enhancement of the oscillator strength for small internal momenta k increases the real part of the exciton continuum contribution substantially below the gap. Above the gap this real continuum part is of the same order of magnitude as below but of different sign. The discrete and the continuum contribution add up constructively below the gap leading to a strongly increased Raman efficiency due to Coulomb correlation (see Fig. 2). Above the gap the discrete and the real part of the continuum contribution have different sign and are roughly of the same order of magnitude. The resulting cancellation makes the total real part of R rather small in the continuum. This destructive interference is also discussed in Ref. 16. Figure 4 shows that the Coulomb correlation tends to diminish somewhat the imaginary part of the Raman tensor. In total, the Coulomb attraction between electron and hole causes a strong asymmetry in the Raman efficiency with respect to the gap, a strong enhancement only occurs below the gap.

The situation for forbidden scattering (Figs. 3 and 5) is similar. Strictly speaking, one cannot distinguish in that case between a discrete and a continuum contribution because of the nondiagonal elements in the internal quantum numbers. It turns out that the part of R due to discrete state only is at least one order of magnitude larger than the total real part in the frequency interval shown in the figures. Below ω_g the cancellation with other contributions in R is incomplete leading to a Raman efficiency which is one to two orders of magnitudes larger than in the free case (see Fig. 3). The total efficiency in the exciton continuum is again of the same order as in the free case because of large cancellations in the real part and the absence of an enhancement in the imaginary part.

Figures 2 and 3 contain experimental values for GaP (Refs. 29 and 30) and CdS.[17,31] In GaP exci-

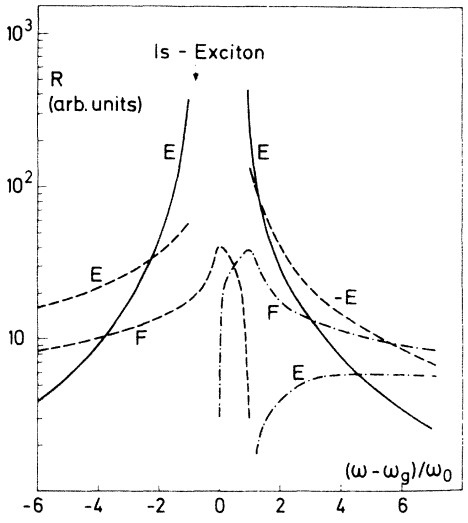

FIG. 4. Different contributions to one of the nonzero components of the Raman tensor for allowed scattering. F dashed curve, real part; F dot-dashed curve, imaginary part with free electron-hole pairs; E solid curve, discrete (real) contribution, E dashed curve, real continuum contribution; E dot-dashed curve, imaginary contribution of Wannier excitons. All contributions have positive sign except of the real continuum contribution of Wannier excitons above the gap, denoted by $-E$.

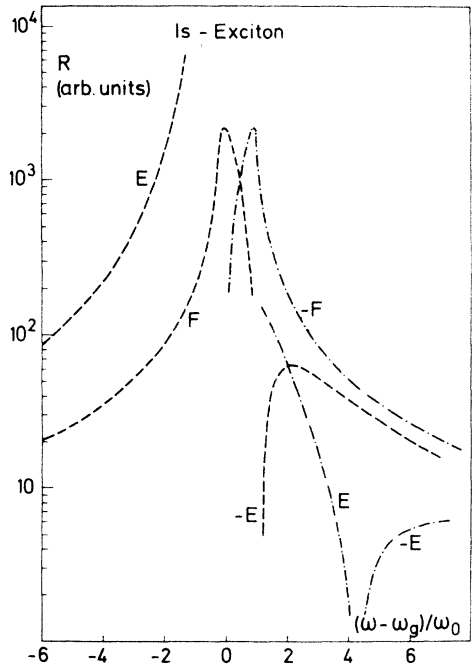

FIG. 5. Different contributions to one of the nonzero components of the Raman tensor for forbidden scattering. F dashed curve, real part; F dot-dashed curve, imaginary part with free electron-hole parts; E dashed curve, real part; E dot-dashed curve, imaginary part with Wannier excitons. The minus sign in front of F or E means that the contribution has a negative sign.

tonic effects are rather small and we compared the experimental scattering efficiencies with theoretical predictions for the free electron-hole case. For CdS the theory with Coulomb correlated electron holes was taken for the comparison.

Figure 2 shows that the agreement between theory and experiment for the uncorrelated case (dashed line) is rather good. The agreement above the gap is still improved if the spin-orbit splitting of the valence bands is taken into account.[30] The theoretical curve for the Coulomb correlated case (solid line in Fig. 2) below the 1s exciton and its comparison with experiment is identical with that of Ref. 19. Above the gap however our curve also contains the imaginary part of the Raman tensor and becomes much flatter (like the experimental points) compared to the curve in that reference. Nevertheless the theoretical values are too low by a factor of about 10 in that frequency region.

Figure 4 shows the same comparison for the forbidden case. The GaP values fit the theoretical curve only for a small frequency region around the gap and then tail off rapidly. A possible explanation for that deviation is that the experimental efficiency also contains allowed scattering contributions due to imperfect experimental conditions or impurities. In any case the experiment does not show a clear violation of the theoretical mirror symmetry of the scattering intensity with respect to the frequency $\omega_g + \frac{1}{2}\omega_0$ (especially if one takes into account the uncertainty in the exact position of the bottom of the conduction band). The figure shows also that the experimental points in CdS of Ref. 31 fit the theoretical curve for the correlated case below the 1s exciton rather well. Above the gap the theoretical curve has a similar slope like the experimental points but it is much too low to explain the experimental efficiency. The large discrepancy in the continuum for CdS is rather puzzling because we treated the exciton-photon coupling exactly and took fully into account the electron-hole correlation. One possibility to explain the discrepancy is that above the gap the radiation does not penetrate deeply into the crystal so that surface effects may play an important role.

APPENDIX: SPATIAL DISPERSION EFFECTS

In this Appendix we shall generalize some of the work of Secs. II and III to include spatial dispersion. We consider allowed scattering and limit ourselves to incident frequencies close to a parabolic 1s exciton band. Assume the crystal is semi-infinite and we are dealing with normal incidence and back scattering. For simplicity we therefore omit the polarization labels γ and γ'.

The work of Sec. II can be taken over directly with the exception of Eqs. (21) and (22). The susceptibility Eq. (21) should now read

$$\chi(\vec{r},\vec{r}') = \begin{cases} \frac{2}{\hbar}\sum_{\lambda s}\frac{g_\lambda \psi_s(\vec{r})\psi_s^*(\vec{r}')g_\lambda^*}{\omega_{\lambda s}^2-(\omega\pm i\eta)^2}, & \text{if } \vec{r} \text{ and } \vec{r}' \text{ are in the crystal region} \\ 0, \quad \text{otherwise.} \end{cases} \tag{A1}$$

Equation (22) now reads

$$\alpha_\lambda(r) = \frac{2i}{\omega}\left(\frac{2\pi}{\hbar}\right)^{1/2}\int d\vec{r}\,'\chi_\lambda(\vec{r},\vec{r}')A(\vec{r}'), \tag{A2}$$

with

$$\chi_\lambda(\vec{r},\vec{r}') = \sum_s \frac{g_\lambda\psi_s(\vec{r})\psi_s^*(\vec{r}')\omega_{\lambda s}^2}{\omega_{\lambda s}^2-(\omega\pm i\eta)^2}. \tag{A3}$$

Equations (A2) and (A3) differ from their counterparts (21) and (22) insofar as the exciton energy $\hbar\omega_{\lambda s}$ now depends on the center-of-mass quantum number s which prevents explicit summation over s at this step. In Ref. 32 an explicit form for $\psi_s(\vec{r})$ was given using as a boundary condition that the boundary is equivalent to an infinitely high repulsive step potential acting on the exciton center-of-mass motion.

Equations (28)–(34) remain valid, but Eq. (35) becomes

$$T_{\vec{k}_0'\vec{q},\vec{k}_0} = 2\sum_{\lambda\lambda'}\frac{f_{\lambda\lambda'}(q)(\omega_\lambda\omega_{\lambda'}+\omega\omega')}{\omega_\lambda^{3/2}\omega_{\lambda'}^{3/2}} \times\int d\vec{r}\,e^{-i\vec{q}\cdot\vec{r}}\int d\vec{r}\,'[\chi_{\lambda'}(\vec{r},\vec{r}')A^{\vec{k}_0'}(\vec{r}')]^{*\text{in}} \times\int d\vec{r}\,''[\chi_\lambda(\vec{r},\vec{r}'')A^{\vec{k}_0}(\vec{r}'')]^{\text{out}}. \tag{A4}$$

In obtaining Eq. (A4) we only considered spatial dispersion to be important in the denominator. The $\vec{r}'$ and $\vec{r}''$ integration can easily be carried out and the result is

$$\int d\vec{r}\,''[\chi_\lambda(\vec{r},\vec{r}'')A^{\vec{k}_0}(\vec{r}'')]^{\text{out}} = g_\lambda\omega_\lambda^2 \times\sum_i\frac{A_i e^{ik_i z}}{\omega_{\lambda k_i}^2-(\omega+i\eta)^2} \tag{A5}$$

for $z \geq 0$, i.e., in the crystal region. We also get the additional boundary condition

$$\sum_i A_i\frac{1}{k_i^2-k_\lambda^{\dagger 2}} = 0. \tag{A6}$$

Here A_i are the vector potential amplitudes of different polarization waves, k_i are the solutions of the dispersion relation

$$\left(\frac{k_i}{k_0}\right)^2 = 1 + \frac{8\pi}{\hbar} \sum_\lambda \frac{|g_\lambda|^2}{\omega^2_{\lambda k_i} - (\omega + i\eta)^2} \tag{A7}$$

and $k_\lambda^\dagger$ is the pole of the denominator of x_λ with positive imaginary part as in Ref. 32. Maxwell's equations give an incident and reflected wave outside the crystal with amplitudes A_{in} and A_{re}, and the boundary conditions

$$A_{\text{in}} + A_{\text{re}} = \sum_i A_i, \quad A_{\text{in}} - A_{\text{re}} = \sum_i \left(\frac{k_i}{k_0}\right) A_i. \tag{A8}$$

The proper normalization for the incident amplitude is

$$A_{\text{in}} = \tfrac{1}{4}\omega\,. \tag{A9}$$

Taking a thermal average over the phonon states and integrating over ω' one obtains for the Stokes component of the total cross section

$$\frac{d\sigma}{d\Omega} = k_0'^3 k_0 \gamma_0 c^2 A'^2 \sum_{i,j=1}^{2} \frac{A_i A_j}{4} \times \frac{F\,\mathrm{Im}(k_i + k_j + 2k')E_i(\omega)E_j(\omega)}{[\mathrm{Re}(k_i - k_j)]^2 + [\mathrm{Im}(k_i + k_j + 2k')]^2}\,, \tag{A10}$$

with

$$E_i(\omega) = \sum_\lambda \frac{|g_\lambda|^2 \omega_\lambda}{\hbar^2} \times \frac{(1 + \omega_\lambda^2/\omega\omega')}{[\omega^2_{\lambda k_i} - (\omega + i\eta)^2][\omega^2_{\lambda k'} - (\omega + i\eta)^2]}\,. \tag{A11}$$

Note that in Eq. (A10) transmission coefficients and absorption are included.

The major result of including spatial dispersion in our treatment is given by Eq. (A10) which should be compared to Eq. (36). There are four contributions in Eq. (A10), three of which arise because of the presence of additional polarization waves [only one term occurs in Eq. (36)]. The terms with $i = j$ are diagonal terms corresponding to incoherent intra- and interbranch scattering; the term $i \neq j$ are interference terms. The latter are very small because $|\mathrm{Re}(k_1 - k_2)| \gg |\mathrm{Im}(k_1 + k_2)|$. The magnitude of the two diagonal term $i = j$ relative to each other depends on the additional boundary condition (A6). Inserting Eq. (A6) into (A10) leads to the result that for equal skin depth, $1/\mathrm{Im}(k_i + k')$, the two diagonal terms $i = j$ give equal contributions to the cross section in a frequency region where both polarization waves can propagate. However, the skin depth $1/\mathrm{Im}(k_i + k')$ always strongly favors the contribution from the mere photonlike branch because the damping of the excitonlike branch is much larger.

It might be worthwhile to point out an important feature of Eq. (A10). In contrast to Eq. (36) the transmission and absorption factors are all contained implicitly in Eq. (A10), whereas they are a separate factor in Eq. (36). Thus, our conclusion is that in general (i.e., when spatial dispersion is included) the scattering cross section does *not* factorize in a naive fashion into a trans-

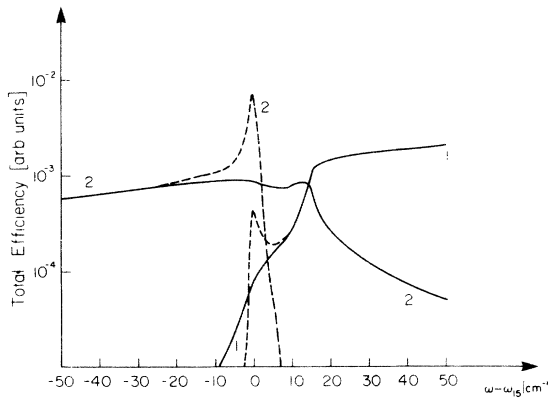

FIG. 6. Contribution from upper (1) and lower (2) polariton branch to the Raman cross section for first-order allowed scattering. Solid line: calculated with spatial dispersion; dashed line: calculated without spatial dispersion. Correction for absorption and reflection are included.

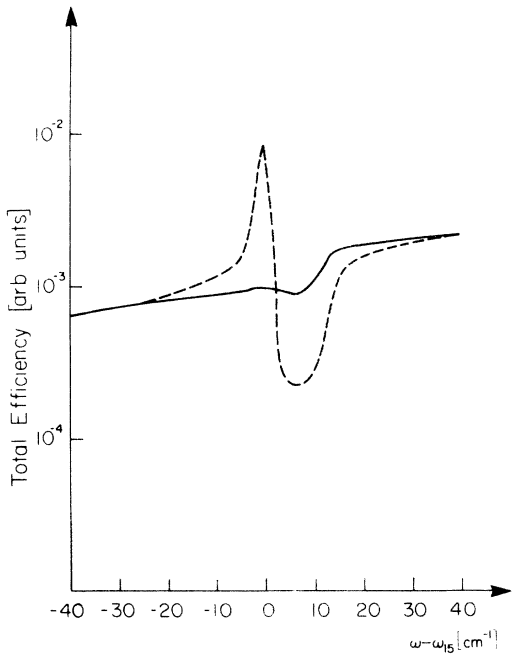

FIG. 7. Sum of both polariton branch contributions to the cross section for first-order allowed scattering. Solid line: calculated with spatial dispersion; dashed line: calculated without spatial dispersion. Correction for absorption and reflection are included.

mission factor times an "internal" cross section.

We have carried out some illustrative numerical calculations based on Eq. (A10), using parameters appropriate for CdS. The values taken were $\omega_{1s} = 20\,700\ \mathrm{cm}^{-1}$; $\Gamma = 1\ \mathrm{cm}^{-1}$; $\epsilon = 8$; $M = 0.9 m_e$; terms $g_{1s}^2 = 1.32 \times 10^4\ \mathrm{cm}^{-2}$. In Fig. 6 the diagonal term ($i = j$) of Eq. (A10) is plotted, including absorption and reflection corrections, as in Eq. (A10). Solid curves included spatial dispersion (and the additional terms), while dashed curves omit it.

These curves indicate two major features. Without spatial dispersion one obtains sharp resonances for the cross section, centered around 0 in Figs. 6 and 7, with halfwidth comparable to the $\Gamma = 1\ \mathrm{cm}^{-1}$ assumed for exciton lifetime. This is smoothed over by including spatial dispersion, as is seen in these figures. Thus a possible test for spatial dispersion would be the absence of sharp lines in the Raman cross section (at low temperatures) where expected, when near the sharp exciton line.

Secondly, our calculation indicates that spatial dispersion effects are small in the sense of not producing sizable extra contributions to the scattering from the additional channels available due to extra propagating polaritons. Only in a frequency region comparable to the longitudinal-transverse splitting of the exciton are these effects even noticeable. The essential point is that the photonlike polariton dominates the scattering and this is essentially the same as if spatial disperson were neglected.

---

*Work supported by the National Science Foundation Grant No. NSF-GH-31742 and Army Research Office-Durham Grant No. DA-AROD-31-124-73-G73. We also acknowledge provision of some free computing time by the University Computing Center, Courant Institute of Mathematical Sciences of New York University.

†Present address: Max-Planck-Institut fur Festkorperforschung, 7000 Stuttgart 1, West Germany.

‡Present address: Department of Physics, Brown University, Providence, R.I. 02912.

§Adress after 1 September 1974: Physics Department, City College of the CUNY, 138th Street and Convent Ave, New York, N.Y. 10031.

[1]R. Loudon, Proc. R. Soc. A 275, 218 (1963).

[2]A. K. Ganguly and J. L. Birman, Phys. Rev. 162, 806 (1967).

[3]D. L. Mills and E. Burstein, Phys. Rev. 188, 1465 (1969).

[4]B. Bendow and J. L. Birman, Phys. Rev. B 1, 1678 (1970).

[5]B. Bendow, Phys. Rev. B 2, 5051 (1970).

[6]J. J. Hopfield, Phys. Rev. 182, 945 (1969).

[7]L. N. Ovander, Fiz. Tverd. Tela 6, 361 (1964) [Sov. Phys.-Solid State 6, 290 (1964)].

[8]L. N. Ovander, Sov. Phys.-Usp. 8, 337 (1965).

[9]A. S. Barker, Jr. and R. Loudon, Rev. Mod. Phys. 44, 18 (1972).

[10]A. Pinczuk and E. Burstein, *Proceedings of the Tenth International Conference on the Physics of Semiconductors*, Cambridge, Mass., 1970, edited by S. P. Keller, J. C. Hensel, F. Stern (U.S. AEC, Div. Tech. Information, Oak Ridge, Tenn. 1970), p. 737.

[11]F. Cerdeira, W. Dreybrodt, and M. Cardona, Solid State Commun. 10, 591 (1972).

[12]V. V. Hizhnyakov, K. K. Rebane, I. J. Techver, *Light Scattering Spectra of Solids*, edited by G. B. Wright (Springer-Verlag, New York, 1969), p. 359.

[13]R. Martin and C. M. Verma, Phys. Rev. Lett. 26, 1241 (1971).

[14]M. V. Klein and P. J. Colwell, *Light Scattering in Solids*, edited by M. Balkanski (Flammarion, Paris, 1971), p. 19.

[15]M. Cardona, in *Proceedings of the Enrico Fermi School Varenna 1971*, edited by E. Burstein (Academic, New York, 1972).

[16]B. Bendow, Phys. Rev. B 4, 552 (1971).

[17]B. Bendow *et al.*, Opt. Commun. 1, 267 (1970).

[18]D. C. Hamilton, Phys. Rev. 188, 1221 (1969).

[19]R. Martin, Phys. Rev. B 4, 3676 (1971).

[20]A. Messiah, *Quantum Mechanics* (Wiley, New York, 1965), Vol. II, p. 807.

[21]M. L. Goldberger and K. M. Watson, *Collision Theory* (Wiley, New York, 1964), p. 202.

[22]A. Messiah, in Ref. 20, p. 828.

[23]W. Brenig, R. Zeyher, and J. L. Birman, Phys. Rev. B 6, 4617 (1972).

[24]R. J. Elliott, Phys. Rev. 108, 1384 (1957).

[25]L. Hostler, J. Math. Phys. 5, 591 (1964).

[26]L. J. Slater, *Confluent Hypergeometric Functions* (Cambridge U. P., Cambridge, England, 1960), p. 51.

[27]I. S. Gradshteyn and I. M. Ryzhik, *Table of Integrals, Series and Products* (Academic, New York, 1965), p. 286, formula 3.197.5.

[28]*Handbook of Mathematical Functions*, edited by M. Abramowitz and I. A. Stegun, Natl. Bur. Stds. Appl. Math. Ser. 55 (U.S. GPO, Washington, D. C., 1964).

[29]J. F. Scott, T. C. Damen, R. C. C. Leite, and W. T. Selfvast, Solid State Commun. 7, 953 (1969).

[30]B. A. Weinstein and M. Cardona, Phys. Rev. B 8, 2795 (1973).

[31]R. H. Callender, S. S. Sussman, M. Selders, and R. K. Chang, Phys. Rev. B 7, 3788 (1973).

[32]R. Zeyher, W. Brenig, and J. L. Birman, Phys. Rev. B 6, 4613 (1972).